Kagomé Compounds

Chandra Shekhar[#], Satya N. Guin, Yan Sun, Enke Liu, Nitesh Kumar, Subhajit Roychowdhury, Tirthankar Chakraborty, Sukriti Singh, Kaustuv Manna, Claudia Felser

Topology combined with broken symmetry gives rise to Weyl semimetals, considering they exist only if the inversion symmetry or time reversal symmetry (TRS) is broken. Although Weyl semimetals with broken inversion symmetry were discovered in the recent past, direct indicators of their broken TRS were elusive. Magnetic Weyl semimetals (WSMs) are expected to exhibit fascinating physical properties, such as the intrinsic and large anomalous Hall effect (AHE). Based on multiple theoretical calculations, single crystal growth, and transport measurements, we proposed a novel topological family comprising the Shandite compounds that exhibit a Kagomé lattice, in which a magnetic WSM $Co_3Sn_2S_2$ was discovered, and this study is the first to do so. The spectroscopic tools revealed the presence of the Fermi arc connecting Weyl points close to the Fermi energy and also revealed the 1D chiral edge states, which are known for the dissipationless current. Additionally, the simultaneous presence of large intrinsic anomalous Hall conductivity and the anomalous Hall angle in bulk $Co_3Sn_2S_2$ leads to high-temperature quantum AHE in $Co_3Sn_2S_2$. This study establishes a magnetic Kagomé lattice WSM as the key material for fundamental research and application in devices that connect topological physics and spintronics.

Topology and crystal symmetry together give rise to a new quantum phase in topological materials. Particularly, honeycomb crystal structures develop the Kagomé lattice, which forms flat bands and frustrated spin structures in magnetic materials. Materials possessing a honeycomb crystal structure are likely to develop exotic states, such as Weyl fermions stemming from the band splitting driven by spin-orbital coupling (SOC), on introducing inversion symmetry or time reversal symmetry breaking into the Kagomé lattice. Although many studies have explored Weyl physics in nonmagnetic materials, studies on magnetic materials are low, and understanding the topological spintronic transport properties in magnetic Weyl semimetals is highly desired, and can be achieved by measuring the electrical and thermal transport properties of Kagomé compounds. Therefore, in this study, we proposed a novel topological family comprising the Shandite compounds that exhibit a Kagomé lattice, in which a magnetic WSM $Co_3Sn_2S_2$ was discovered. To the best of our knowledge, this study is the first to explore magnetic compounds in a Kagomé lattice.

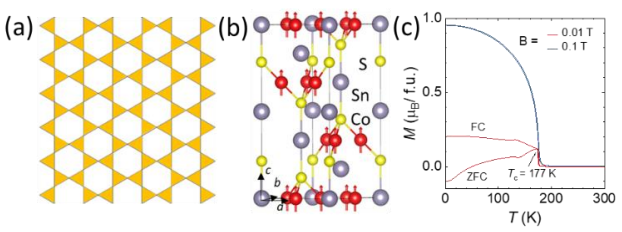

Fig. 1: (a) Representation of the Kagomé lattice wherein magnetic or non-magnetic atoms are arranged in a hexagonal structure along c-axis, (b) Unit cell of $Co_3Sn_2S_2$ where Co atoms form the Kagomé lattice, and (c) Temperature-dependent magnetization of $Co_3Sn_2S_2$, showing ferromagnetic Tc.

Materials belonging to the Kagomé lattice family. There are several space groups in which atoms form Kagomé lattice. Fig. 1a shows a typical representation of the Kagomé lattice derived from a honeycomb structure, wherein each Kagomé triangle comprises a honeycomb site, and each honeycomb bond comprises one Kagomé site. $Co_3Sn_2S_2$ belongs to the Shandite family and is the only ferromagnet with a Curie temperature of 177 K (Fig. 1c). In the crystal structure of $Co_3Sn_2S_2$, Co atoms are arranged in a Kagomé triangle (Fig. 1b), and due to their spin direction, Co atoms align along *c*-axis, giving rise to a magnetic moment of 0.29 μ_B/Co. Additionally, due to extremely strong magnetic anisotropy, $Co_3Sn_2S_2$shows a quasi-two-dimensional (2D) nature with an out-of-plane magnetization.

Large, intrinsic anomalous Hall conductivity derived from Berry phase. In this study, we measured the field-dependent Hall resistivity of $Co_3Sn_2S_2$ along the different crystal axes by experiments. It was observed that $Co_3Sn_2S_2$ exhibited anomalous behavior when the magnetic field was applied along the *c*-axis. Consequently, the corresponding anomalous Hall conductivity (σ_H) was calculated as 1130 Ω^{-1} cm^{-1} at 2 K (Fig. 2a), which is in close agreement with the theoretical values calculated using the Kubo formula. Moreover, the obtained value for σ_H remained constant up to 100 K, while simultaneously being independent of the longitudinal conductivity (Fig. 2b), which was rare in T_c materials, thereby indicating that the intrinsic origin of anomalous Hall conductivity was based on

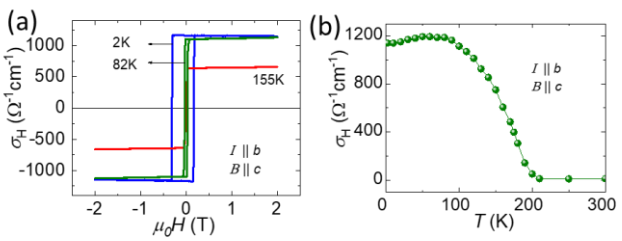

Fig. 2: (a) Measured anomalous Hall conductivity (AHC) at the specified temperatures, and (b) Temperature dependent AHC.

the unified scaling model and is dominated by the Berry curvature in momentum space. By integrating Berry curvature in the Brillouin zone (BZ) for the occupied states, σ_H remained constant above 1000 Ω^{-1} cm^{-1} within 100 meV around E_F. The DFT calculations were consistent with the observed scaling behavior, which further verifies the Weyl phase in $Co_3Sn_2S_2$. Additionally, $Co_3Sn_2S_2$ exhibited a maximum anomalous Hall angle of ~20% around 120 K.

Zero-field anomalous Nernst effect. In ferromagnetic materials like $Co_3Sn_2S_2$, internal magnetization induces additional electric voltage orthogonal to the applied temperature gradient, which is referred to as the anomalous Nernst effect (ANE). Therefore, we investigated the dependence of the Nernst thermopower (S_{xy}) on the magnetic field at different temperatures (Fig. 3a). As a result, the ANE behavior of S_{xy} was observable up to T_c, but increased to approximately 3 μV/K at 82 K. The estimated temperature dependent on the anomalous transverse thermoelectric conductivity from S_{xy} increases gradually as the temperature increases up to T_c. While the S_{xy} of soft magnetic material is zero once the magnetic field is eliminated, a non-zero value of S_{xy} is observed for hard-magnetic materials, such as $Co_3Sn_2S_2$. Therefore, we magnetized the $Co_3Sn_2S_2$ sample by applying a magnetic field of ±1 T, which is greater than its saturation field, to align the magnetic moments along the *c*-axis, and then switched off the magnetic field. Fig. 3b represents ANE of $Co_3Sn_2S_2$ in zero magnetic fields as a function of temperature, which increases as the temperature increases, and reaches a peak value of 3 μV K^{-1} at 80 K. Any further increase in the temperature leads to a decrease in ANE, and above 120 K, the signal is nearly zero considering the compound loses its hard-magnetic structure. Therefore, we can conclude that the observed maximum value is remarkable considering the magnetic moment of $Co_3Sn_2S_2$.

Discovery of magnetic Weyl. Over the past decade, there has been a lot of progress on non-magnetic Weyl semimetals. Although a series of magnetic materials that break time reversal symmetry (TRS) and exhibit Weyl points has been predicted, they have never been realized. Additionally, these materials host emergent Weyl fermions in the bulk and surface Fermi arc states that connect the Weyl points having opposite chirality.

Angle-resolved photoemission spectroscopy. The TRS-breaking WSM phase in $Co_3Sn_2S_2$ is caused by the crystal field, ferromagnetism, and SOC. The crystal field first combines the valence and conduction bands to form fourfold degenerate nodal lines. Based on our density functional theory calculations, six nodal rings of linear crossings were revealed in the spin-up channel based on the band inversion. When the SOC of the nodal rings was gapped, three pairs of Weyl nodes located 60 meV above the charge neutrality point were formed (Fig. 4a, top), which was much closer to the Fermi energy E_F than that of the previously proposed magnetic WSMs. These Weyl nodes and non-trivial Weyl nodal rings combined result in a clean topological band structure around the E_F, which further enhances the Berry curvature in the Brillouin zone.

Our recent study on angle-resolved photoemission spectroscopy of $Co_3Sn_2S_2$ revealed the existence of surface Fermi arcs (SFAs) around the $\bar{K}$ band of the BZ formed by a line segment connecting one pair of Weyl points to the opposite chirality in each BZ (Fig. 4a, bottom). The line segments originating from three adjacent BZs forms a triangle, and this unusual surface FS topology exhibiting different photon energies indicates the surface origin of the SFAs. Notably, each line-segment FS piece merges into the bulk FS pockets near the $\bar{M}$ point of the BZ, where the Weyl points are located. On measuring the SFAs, the measured bulk band dispersion was found to be linear, considering the

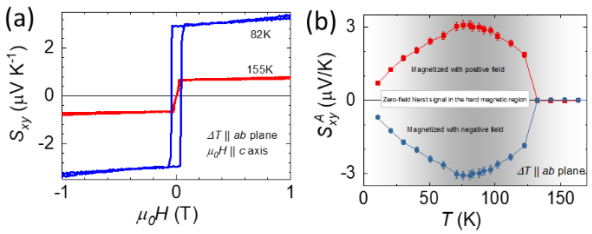

Fig. 3: (a) Magnetic field dependence of the Nernst thermopower S_{xy} at different $Co_3Sn_2S_2$ temperatures, and (b) Temperature dependent anomalous Nernst effect (ANE) of $Co_3Sn_2S_2$ in zero field.

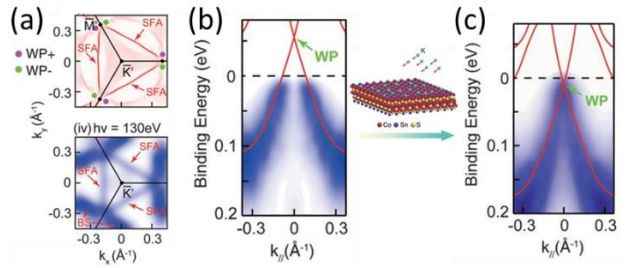

Fig. 4: (a) (top) The calculated Fermi surface (FS) where the surface Fermi arc (SFA) is indicated by red arrows. (bottom) The experimentally observed FS, (b) Band dispersion showing linear dispersions in the direction of the Weyl point above E_F, and (c) After in situ electron doping using potassium metal.

Weyl points were located at an energy level of approximately 50 meV above E_F for the pristine sample (Fig. 4b). Furthermore, to observe the band crossing that carries the Weyl points in $Co_3Sn_2S_2$, we introduced in situ electron doping using potassium metal dozer and successfully raised E_F (Fig. 4c).

Scanning tunneling spectroscopy. The electron states, particularly, the real-space patterns created by the interference of electrons, can be measured with the atomic resolution using scanning tunneling spectroscopy. Hence, topologically protected and non-protected electronic properties of Weyl semimetals can be resolved using scanning tunneling spectroscopy. As mentioned above, $Co_3Sn_2S_2$ forms Kagomé lattice along the *c*-axis, and its layered structure enabled us to analyze all the three terminations of the (001) surface (Fig. 5a). The single crystals of $Co_3Sn_2S_2$ were cold cleaved at 80 K under ultrahigh-vacuum conditions and measured at 4.2 K. The most favorable cleave plane was observed between the Sn and S atomic layers, and most of the cleaved surfaces exhibited a triangular atomic structure, indicating the presence of the Sn or S termination. However, the probability of the presence of Sn or S termination was very rare to detect at the Co terminal, charactering the Kagomé lattice. The key observations were that the arcs connected different Weyl points based on the chemical composition of the topmost surface of $Co_3Sn_2S_2$. Besides, to visualize the Fermi arcs and explore their energy evolution capabilities on the various surface terminals, we measured the quasiparticle interference (QPI) patterns that elastically scattered electrons embed into the local density of states (LDOS) measured using differential conductance (d*I*/d*V*) maps.

The QPI patterns of the Sn surface generally have sharp polygonal shapes. However, in the representative QPI map taken at 7.5 meV, as shown in Fig. 5b, the QPI pattern exhibited a hexagonal shape around $q = 0$ with its replicas centered on Bragg peaks. The corresponding calculated surface density of states DOS(*k*) of the Sn termination is shown in Fig. 5c. We found that the hexagonal QPI pattern originated from the scattering between a buckled hexagonal electron pocket around Γ and the adjacent edges of buckled triangular electron pockets at the *K* and *K′* corners of the BZ formed by the open-contour Fermi-arc bands, and each edge connects a pair of Weyl cones within the BZ. Furthermore, depending upon the types of surface termination, the distinct surface potentials imposed by three different terminations resulted in modified Fermi-arc contour and Weyl node connectivity. On the Sn terminal, the Weyl node connectivity of Fermi arcs was in the intra–Brillouin zone, whereas on the Co terminal, it was adjacent to the Brillouin zone. On the S surface, Fermi arcs overlap with nontopological bulk and surface states. These findings suggest that the competent layout of multiple surface terminations can be used to manipulate topological current in circuits.

Observation of 1D chiral edge states. The physical realization of Chern insulators has been predicted to host the quantum anomalous Hall effect (QAHE) and topologically protect the chiral edge states that carry dissipationless current, and hence, is of fundamental and practical interest. Such edge states have recently been discovered in $Co_3Sn_2S_2$ using a scanning tunneling spectroscope. Depending on the interlayer coupling strength, the chiral edge states can be localized on partially exposed Kagomé planes on the surfaces of a Weyl semimetal. Additionally, our d*I*/d*V* maps on the Kagomé Co_3Sn terraces show the topological states confined to the edges, which display linear dispersion in the opposite direction of the conventional quantum well states originated from free-electron-like quadratic dispersion. The nature of the

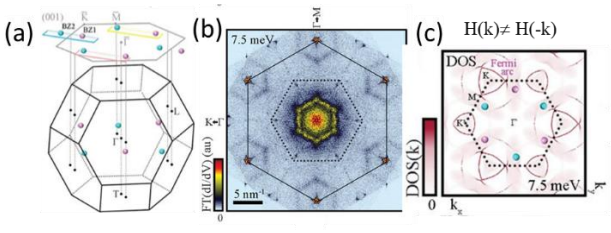

Fig. 5: (a) Bulk BZ hosting three pairs of Weyl nodes and their (001) surface projection, (b) Fourier transform of two dI/dV maps at 7.5 meV and 4.2K, depicting sharp QPI patterns, and (c) ab-initio calculated DOS(k), showing Fermi arcs and surface-projected bands.

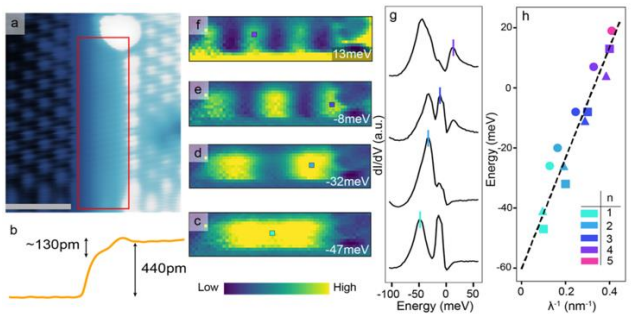

Fig. 6: (a) Topography of a step edge between two S surfaces comprising a small terrace of the Co_3Sn plane, indicated by the red rectangle, (b) Line profile of the step edge, (c–f) The density of state maps of the region enclosed by red rectangle in a, (g) Spectra at high density of states locationsfor each quantum well-like state indicated by small squares in c–f, and (h) Energy versus inverse wavelength relation for states found on three Co_3Sn terraces.

chiral edge states has been explored further. A partial cleavage between the Sn surface that is approximately 130 pm below the S surface occasionally leaves the small terraces near step edges on the S surface (Fig. 6a and b). However, the closest plane to the S surface is the Co_3Sn plane located 156 pm below the Sn surface, with the next plane at 312 pm. Thus, the thin terrace can be unambiguously identified as the Co_3Sn plane. The d*I*/d*V* map of these terraces revealed a quantum well-like bound states at various energies, as shown in the DOS images (Fig. 6c–f), which can be identified from the peaks in the spectra at locations where the density of states is maximum (Fig. 6g). For a 5.2 nm terrace (Fig. 6a), we observed a sequence of four quantum well-like states ranging from n = 1 to n = 4, where n indicates a bound state with n+1 nodes and n maxima in the local density of states, and the notation for the nth state is the same as that in the classic quantum well. Unlike the conventional quantum well, the dispersion seen on all the terraces observed is linear (Fig. 6h), thereby confirming the 1D nature of chiral edge states.

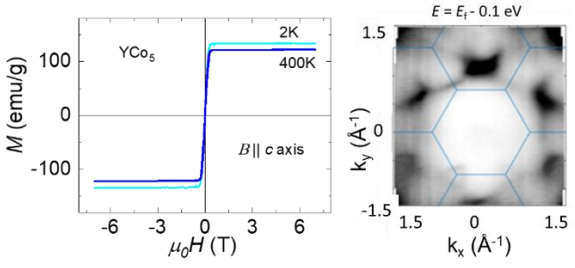

Fig. 7: (left) Field depedent magnetization of YCo_5. (right) Angle resolved photoemission spectra of YNi_5.

Future direction. The Kagomé lattice is known to have a flat band, and the charged particles exhibit infinite mass that freezes their kinetic energy, and this high degenerated state forms an ideal platform to achieve strongly correlated electronic states, such as superconductivity, fractional quantum anomalous Hall effect, excitonic insulator state, and magnetism. Although many such materials exist in various space groups, the flat band properties have not been demonstrated due to the lack of materials. For further study, we scrutinized the materials from various space groups. For example, we conducted preliminary investigations of space group 191 (YCo_5, YNi_5) to analyze the correlation between the electronic structure and intriguing physical behavior of the materials.

Conversely, $Co_3Sn_2S_2$ possesses quasi-2D Co_3Sn layers that exhibit chiral edge states, which leads to the emergence of quantum AHE in the 2D nature. Therefore, $Co_3Sn_2S_2$ is one of the promising materials to exhibit high temperature quantum AHE.

References

[1]* *Giant anomalous Hall effect in a ferromagnetic Kagomé-lattice semimetal, E. Liu, Y. Sun, N. Kumar, L. Müchler, A. Sun, L. Jiao, S. Y. Yang, D. Liu, A. Liang, Q. Xu, et al., Nat. Phys.* ***14*** *(2018) 1125-1131.*

[2]* *Zero-Field Nernst effect in a ferromagnetic Kagome-lattice Weyl-semimetal $Co_3Sn_2S_2$, S. N. Guin, P. Vir, Y. Zhang, N. Kumar, S. J. Watzman, C. Fu, E. Liu, K. Manna, W. Schnelle, J. Gooth, et al., Adv. Mater.* ***31*** *(2019) e1806622.*

[3]* *Magnetic Weyl semimetal phase in a Kagomé crystal, D. F. Liu, A. J. Liang, E. K. Liu, Q. N. Xu, Y. W. Li, C. Chen, D. Pei, W. J. Shi, S. K. Mo, P. Dudin, et al., Science* ***365*** *(2019) 1282-1285.*

[4]* *Fermi-arc diversity on surface terminations of the magnetic Weyl semimetal $Co_3Sn_2S_2$, N. Morali, R. Batabyal, P. K. Nag, E. Liu, Q. Xu, Y. Sun, B. Yan, C. Felser, N. Avraham, and H. Beidenkopf, Science* ***365*** *(2019) 1286-1291.*

[5] *Evidence for 1D chiral edge states in a magnetic Weyl semimetal $Co_3Sn_2S_2$, S. Howard, L. Jiao, Z. Wang, N. Morali, R. Batabyal, P. K. Nag, N. Avraham, H. Beidenkopf, P. Vir, C. Shekhar, Nature Communications* ***12*** *(2021) 4269, arXiv:1910.11205 (2019).*

[6] *Massive Dirac fermions in a ferromagnetic kagome metal, L. Ye, M. Kang, J. Liu, F. von Cube, C. R. Wicker, T. Suzuki, C. Jozwiak, A. Bostwick, E. Rotenberg, D. C. Bell, et al., Nature* ***555*** *(2018) 638-642.*

[#] shekhar@cpfs.mpg.de